CHAPTER 6

NON-EQUIATOMIC $Fe_{40}Cr_{25}Ni_{15}Al_{15}Co_5$ HIGH-ENTROPY ALLOY

The extensive review of HEAs literature suggests that these alloys are potentially attractive for their ability to form simple solid solution phases, i.e. body centered cubic (BCC), face centered cubic (FCC) and hexagonal close-packed (HCP), primarily due to the high entropy effect. However, in the recent reports, the effect of high-entropy is the most debated parameter of HEAs as only a small fraction of alloys fulfil the composition requirement for simple solid solution formation, and many HEAs have been reported with multiple phases and complex microstructures [14]. It has been observed that the formation of intermetallic phases is more frequent than simple solid solutions in HEAs, and the secondary phases contribute to the alloy properties significantly [152]. A Ni-based superalloy, where gamma (FCC) matrix is composed of cuboidal gamma prime ($L1_2$) precipitates is the best example. These alloys are known to have interesting properties, i.e. high strength at elevated temperature etc. Similar to this special class of alloys, HEAs are also reported to have a good combination of properties due to the formation of B2 and $L1_2$ phase within the BCC and FCC matrixes [152]. Formation of the B2 phase has been observed in a large number of equiatomic or non-equiatomic HEAs as a major or minor phase [120]. Ma et al. [153] have reported the formation of cuboidal nano precipitates in BCC HEAs based on the $Al_2(NiCoFeCr)_{14}$ composition and determined the factors affecting the formation of the B2 precipitates. The effect of these precipitates on the mechanical properties has been discussed by following the strengthening mechanism. In some cases, the formation of the B2 phase is reported during heat-treatment of HEAs [119]. Moreover, it was observed that the alloys

containing Fe, Co, Ni, along with Al, showed a strong affinity to form B2 phase. Formation of the B2 phase along with Fe-Cr rich disordered BCC phase has been reported more frequently in AlCrFeCoNi HEA system [154].

This chapter deals with a non-equiatomic AlCrFeCoNi HEA processed through induction melting (IM). The present investigation is aimed at developing precipitation hardened (superalloy like alloys) iron-rich non-equiatomic $Fe_{40}Cr_{25}Ni_{15}Al_{15}Co_5$ high-entropy alloy. In addition to that, the effect of configurational entropy (ΔS_{conf} = 11.90 J/K mol, ~ 11% lower than the equiatomic AlCoCrFeNi HEA) on phase formation is also intended to be explored. The phase evolution, thermal stability and mechanical properties of the alloy are investigated.

6.1 Structural evolution

The X-ray diffraction patterns of $Fe_{40}Cr_{25}Ni_{15}Al_{15}Co_5$ alloy in as-cast condition and after heat-treatment at 600 ºC (873K) and 900 ºC (1173K) for 2h are displayed in Fig. 6.1. The as-cast sample showed the formation of a two-phase structure of ordered B2 and a BCC phase. The formation of the ordered phase is confirmed through the presence of the superlattice reflection (100) diffraction peak. The average lattice parameters of B2 & BCC phase are 2.88±0.02, 2.87±0.01 respectively in the as-cast condition. The heat-treated sample at 873K exhibits the similar phase constitution of B2 and BCC phase. The only noticeable change is the decrease in the intensity of the characteristic peak (100) of the B2 phase, along with the appearance of other peaks (211), (200). The (110) peak is showing a higher intensity compared to that of the as-cast alloy. This infers that the volume fraction of the BCC phase has increased after heat-treatment at 873K. On further increase in heat treatment temperature at 1173K, no change in the phase constituents was observed.

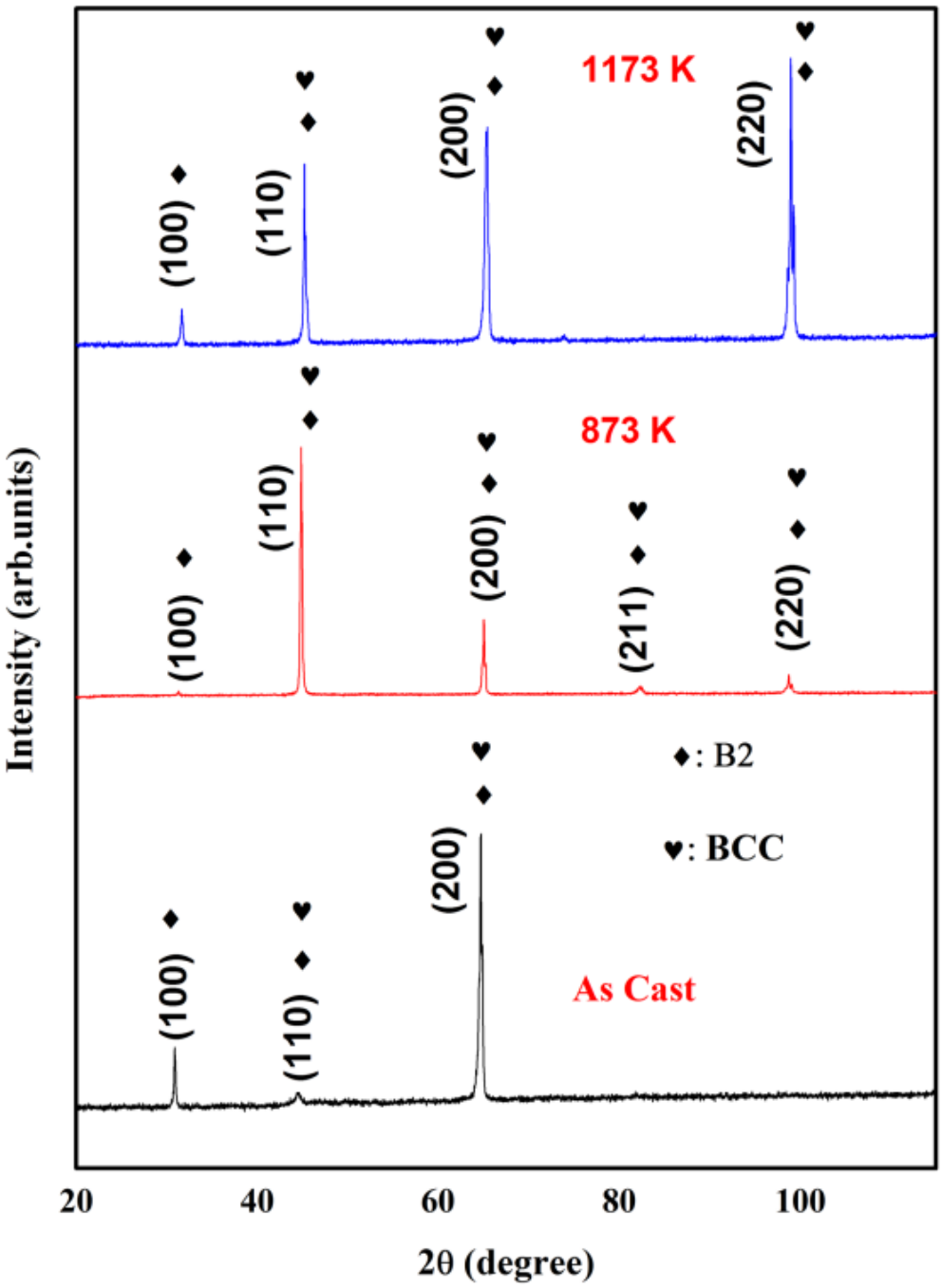

Figure 6.1: X-ray diffraction patterns of $Fe_{40}Cr_{25}Ni_{15}Al_{15}Co_5$ HEA in as-cast and heat-treated conditions at 600 ºC (873K) and 900 ºC (1173 K) for 2h. Evolution of the two-phase structure of (B2+BCC) could be discerned.

6.2 Microstructural evolution

The microstructural evolutions of the as-cast and heat-treated samples were investigated by optical microscopy (OM) and scanning electron microscopy (SEM).

Fig. 6.2 depicts the optical micrographs of the as-cast, and the heat-treated samples annealed at 873 K and 1173 K for 2h followed by water quenching. As-cast alloy exhibits the formation of columnar dendritic microstructure (figure 6.2(a)).

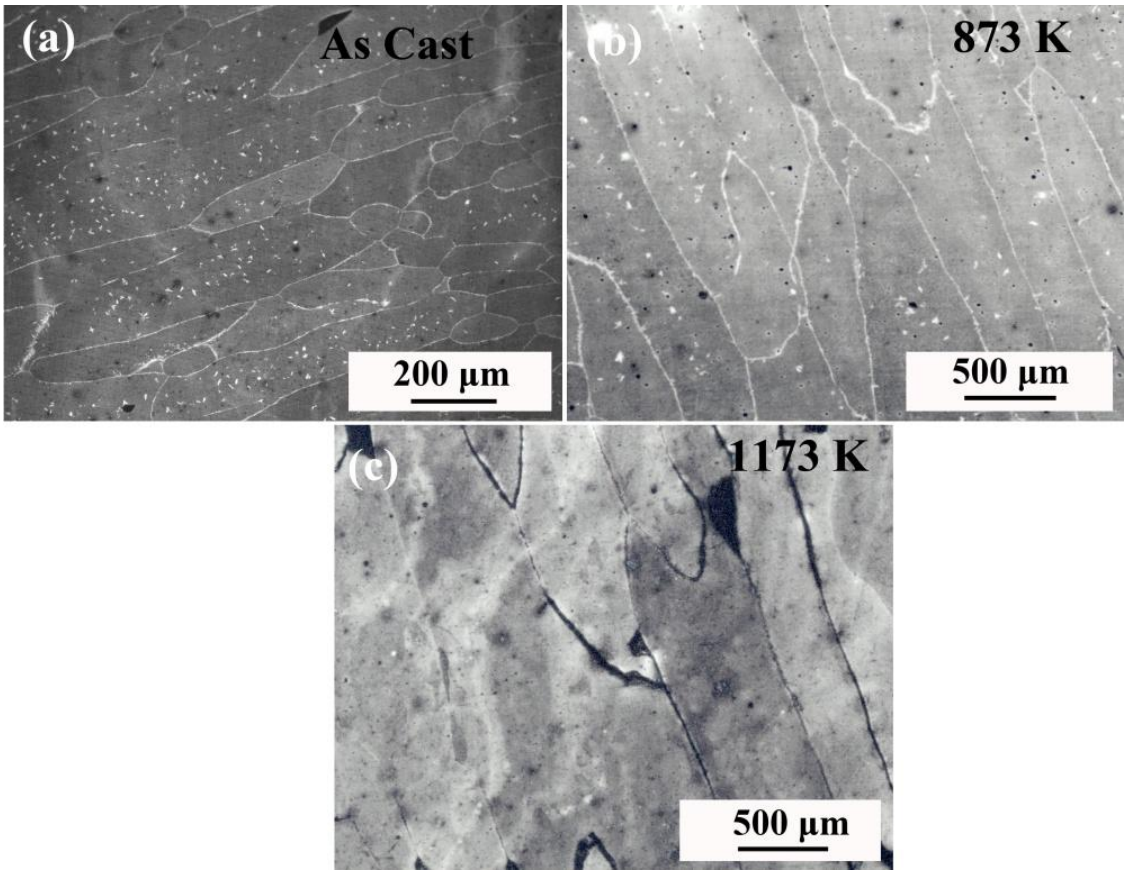

Figure 6.2: The optical micrographs of $Fe_{40}Cr_{25}Ni_{15}Al_{15}Co_5$ high-entropy alloy in (a) as-cast and heat-treated conditions of (b) 600 ºC (873K) (c) 900 ºC (1173K) for 2h, respectively. Columnar dendrites could be observed in all micrographs.

The width of columnar dendrites is varying in the range of 50 to 100µm in the as-cast state. It has been observed that the heat-treated samples retained the columnar dendritic structure even at 873 K and 1173 K respectively. However, the change in the size of columnar dendrites could be observed as the temperature increases. For a better

understanding of the morphological changes in these samples, backscattered imaging (BSE) was carried out. The SEM-BSE micrographs are represented in Fig.6.3.

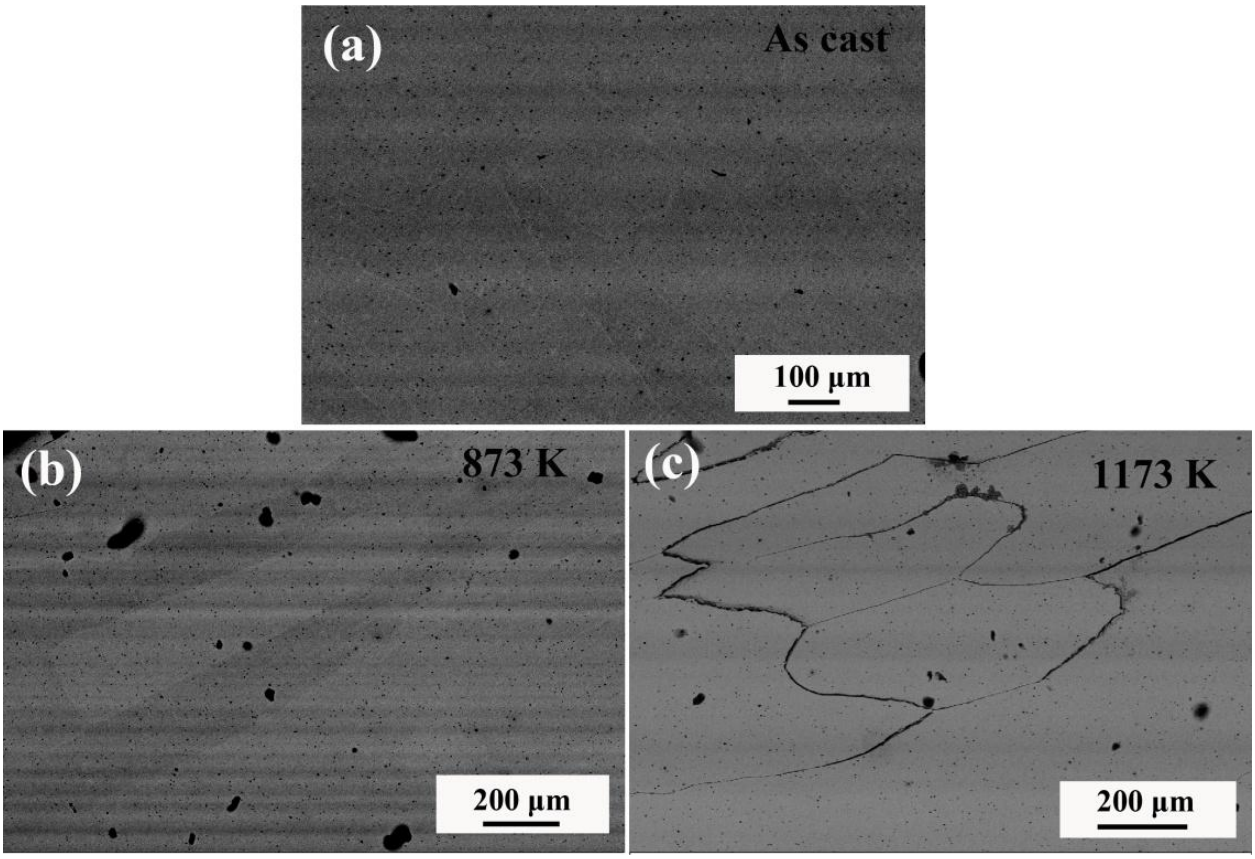

Figure 6.3: The SEM micrographs of $Fe_{40}Cr_{25}Ni_{15}Al_{15}Co_5$ high-entropy alloy in (a) as-cast and heat-treated conditions of (b) 873K (c) 1173K for 2h followed by water quenching.

No clear phase contrast was observed in the as-cast sample. However, the coarser columnar dendrites are visible in the sample. The heat-treated sample at 873K showed the two-phase morphology. The darker contrast is richer in Ni-Al and grey contrast in Fe-Cr elements. It confirms the formation of coherent B2 and BCC microstructure. The similar features were observed in the heat-treated sample annealed at 1173 K. Coarsening of the columnar dendrites were detected as the temperature of heat-treatment increases. In all these micrographs, the presence of impurity was noticed in the form of oxides and

carbides. The presence of the impurity could not be ruled out because melting was done in the open atmosphere.

The chemical compositions of the constituent microstructural features were analyzed using SEM-EDS full frame analysis, and results are listed in Table 6.1. The experimental results are justifiable to the initial compositions of the constituent elements.

Table 6.1: The chemical composition of the constituent elements in as-cast $Fe_{40}Cr_{25}Ni_{15}Al_{15}Co_5$ high-entropy alloy.

Elements	FeK	CrK	NiK	AlK	CoK
Atomic % (calculated)	40	25	15	15	5
Atomic% (experimental) Error - (±5%)	40.7	26.8	13.3	14.8	4.5

In order to examine the two-phase nature of the BCC/B2 matrix, the transmission electron microscopy (TEM) analysis was performed. The bright field and corresponding selected area diffraction (SAD) pattern of the as-cast alloy are given in Fig. 6.4. It could be demonstrated form the bright field imaging (Fig. 6.4 (a)) that cuboidal B2 precipitates are present uniformly in the BCC matrix. These cuboidal B2 precipitates of sizes 100-200 nm are embedded with the in the disordered BCC matrix. In the diffraction pattern cubic pattern with a four-fold rotation symmetry is easily discerned. Modulation of intensity among the diffraction spots are present which may be due to the partial or complete ordering of either B2/BCC phase or both phase simultaneously. Whatever may be the situation, there is a strong orientated relationship between the phases. The orientation relationship is [100] of B2 phase is parallel to the [100] of BCC phase and the [110] of

the B2 phase is parallel to the [110] of BCC phase. This is commonly known as cube-on-cube orientation relationship with no in-plane rotation. Under this situation, the interface between the cuboid and the matrix is likely to be (100) type.

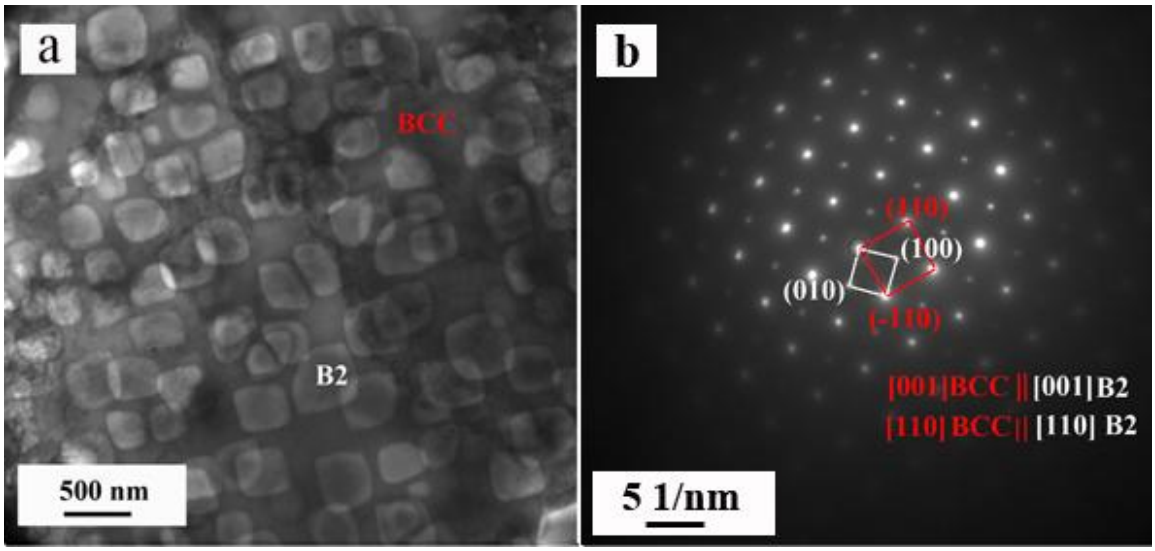

Figure 6.4: The transmission electron micrograph and selected area diffraction pattern (SAD) of as-cast $Fe_{40}Cr_{25}Ni_{15}Al_{15}Co_5$ HEA (a-b). Cuboidal B2 precipitates coherently embedded in BCC disordered matrix.

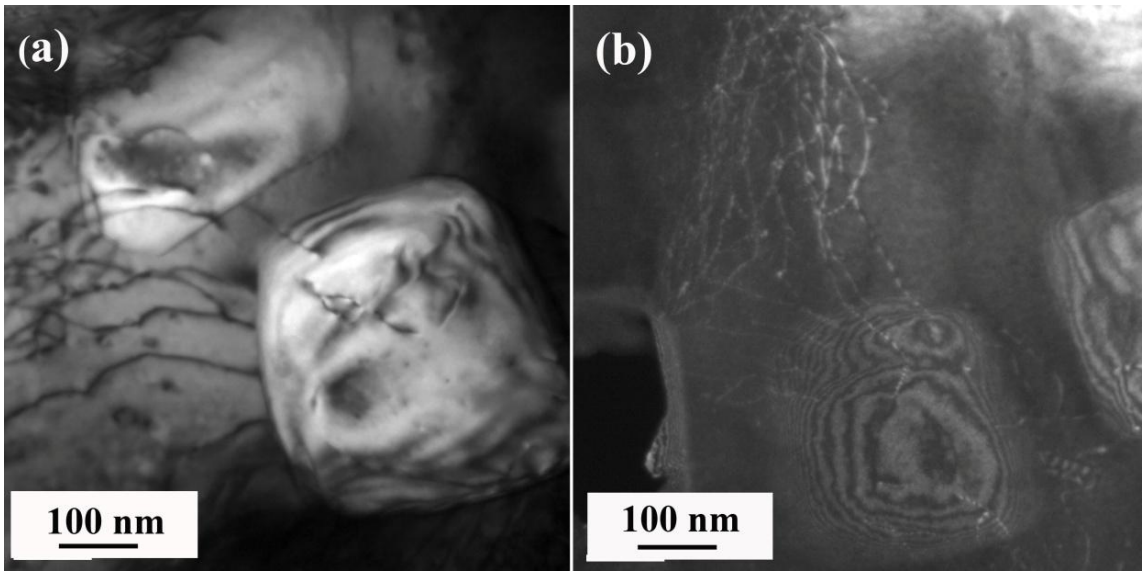

Figure 6.5: The magnified view of bright and dark field images (a&b) of B2 precipitate with disordered BCC matrix.

A closer view of the B2 precipitate with BCC matrix can be seen through magnified images reported in Fig. 6.5. Fig. 6.5 (a&b) shows the bright field and dark field image of

the B2 precipitate with the matrix. Presence of the dislocation lines could be observed in the bright field image. Some of the dislocations are passing through the matrix, which helps in understanding the some sort of coherency between the BCC and B2 phase.

6.3 Chemical composition

The elemental distribution with compositional information of the as-cast HEA was analyzed through STEM-EDS mapping (Fig. 6.6).

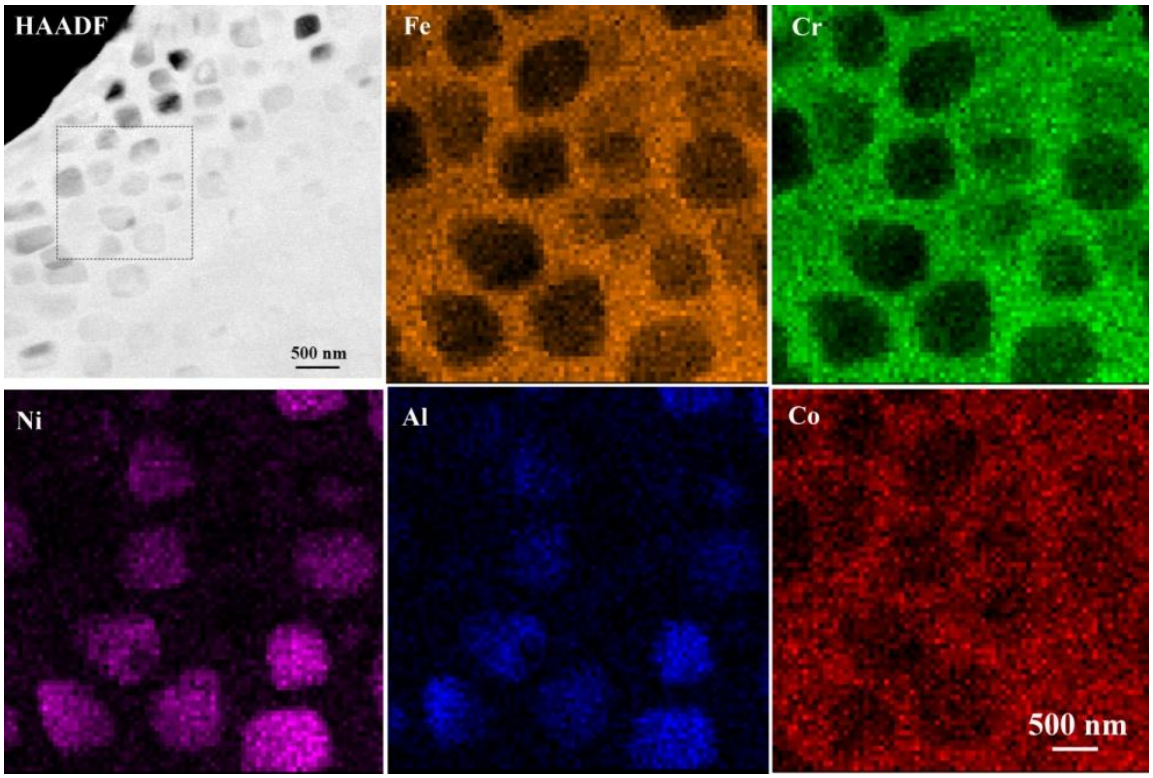

Figure 6.6: The STEM-EDS mapping of as-cast $Fe_{40}Cr_{25}Ni_{15}Al_{15}Co_5$ high-entropy alloy. Cuboidal B2 precipitates could be seen richer in Ni-Al and matrix BCC in Fe-Cr elements. Co is homogeneously distributed in the alloy.

It has been found that Fe and Cr elements are richer in the matrix, and cuboidal precipitates are enriched in Al and Ni. Cobalt (Co) appears to be homogeneously distributed across the precipitate & the matrix. It further helps in substantiating the fact that the matrix is rich in Fe and Cr and of BCC structure and precipitates are more likely

Al-Ni rich B2 type ordered phase. Co is almost homogeneously present in the BCC matrix and in the B2 cuboidal phase. Even though the B2 phase appears to be ordered, some amount of Co has diffused into it, and most likely it has substituted the Ni-site in the lattice leading to partially ordered structure. The compositional line profile analysis also supports the formation of ordered –disordered transformation in the present alloy. Fig. 6.7 showed similar behaviour of compositional variation of cuboidal B2 precipitates that are enriched in Ni & Al elements and the matrix is rich in Fe and Cr.

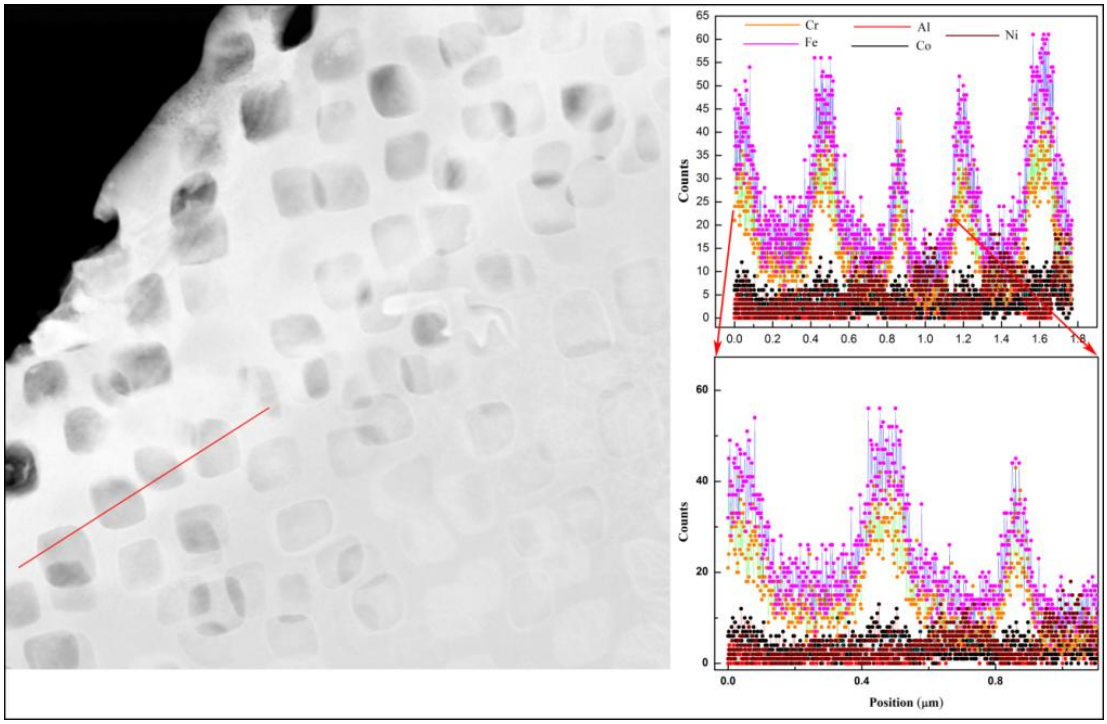

Figure 6.7: The line profile analysis of as-cast $Fe_{40}Cr_{25}Ni_{15}Al_{15}Co_5$ high-entropy alloy (HEA).

6.4 Thermal stability

In order to understand the thermal stability of the alloy, differential scanning calorimetry (DSC) was conducted of as-cast alloy. The DSC thermogram of the as-cast $Fe_{40}Cr_{25}Ni_{15}Al_{15}Co_5$ HEA is given in Fig. 6.8. It could be observed that no major heat

evolution event is occurring in the alloy. However, an indication of the exothermic event, which ranges in between 400 ºC to 600 ºC (673K- 873K) could be observed. This might be the reflection of the structural variation in the alloy.

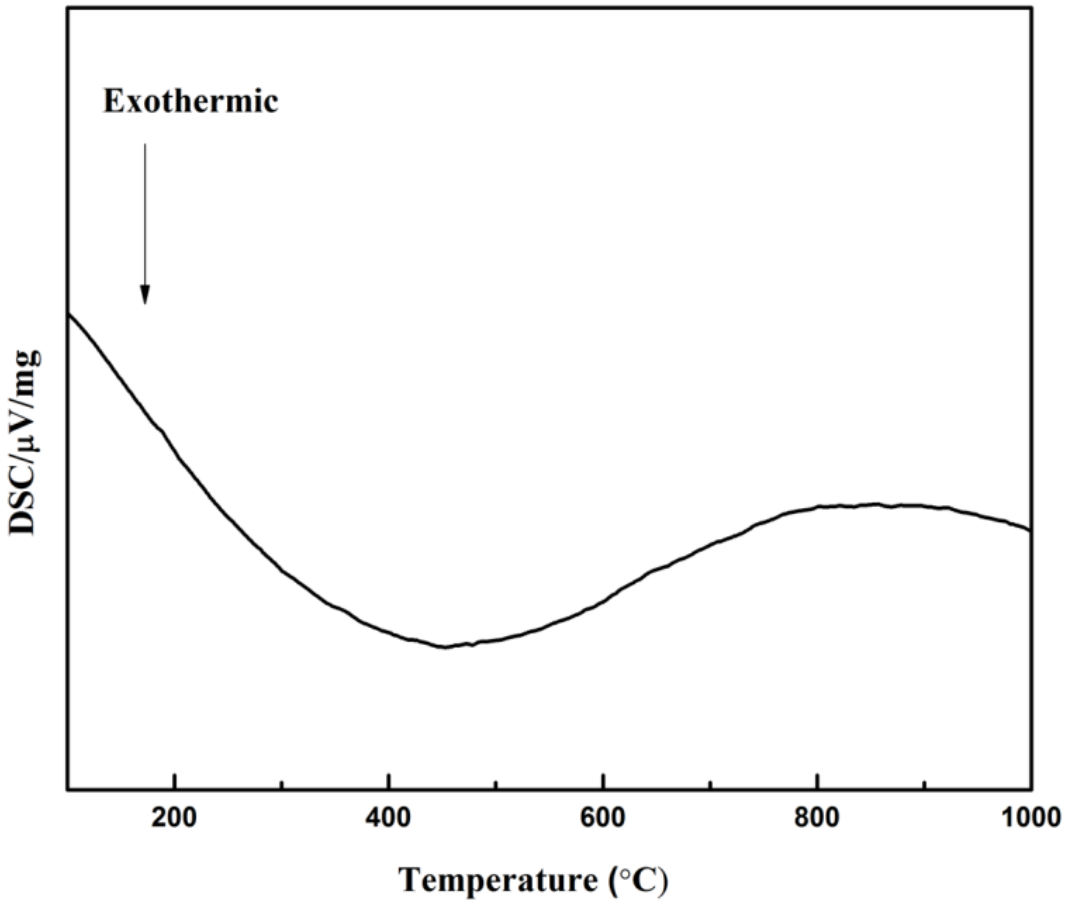

Figure 6.8: The dynamic differential scanning calorimetric (DSC) thermogram of as-cast $Fe_{40}Cr_{25}Ni_{15}Al_{15}Co_5$ HEA. No major heat event is observed. Wide exothermic peak over a range of temperature is attributing to grain growth.

To further substantiate this exothermic event, heat treatment of the alloy was conducted at 873 K, 1173K for 2h and at 1073K for longer holding time of 12h followed by furnace cooling. The X-ray diffraction patterns of the heat-treated samples along with as-cast alloy have been given in Fig. 6.9.

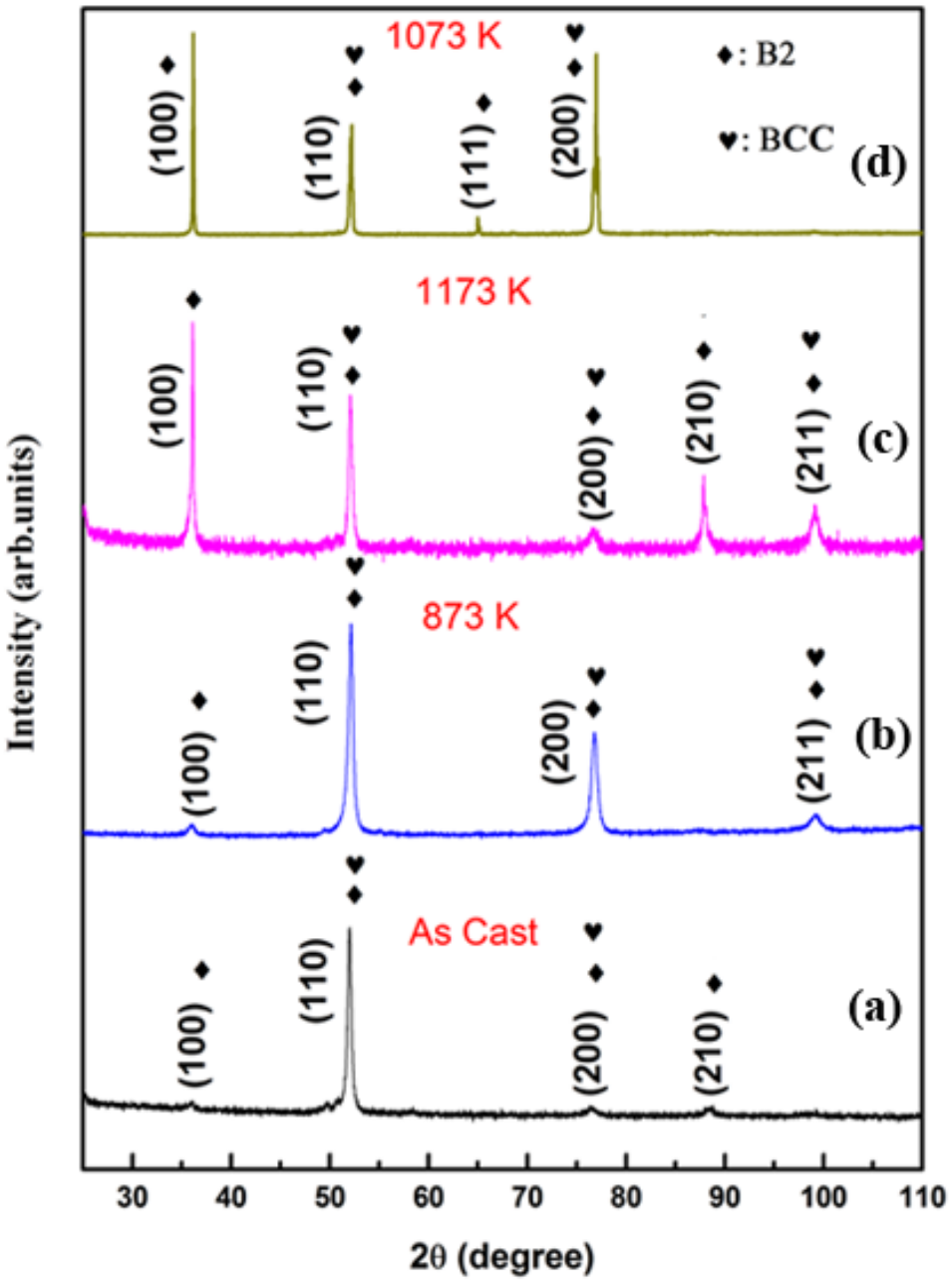

Figure 6.9: X-ray diffraction patterns of (a) as-cast and (b) heat-treated samples at 600 ºC (873K), 900 ºC (1173 K) - 2h & 800º C (1073 K) for 12h and cooled down in a furnace. Evolution of similar types of phase could be observed in all conditions.

It can be seen that at 600 ºC (873K) there was no change in the phase that could be observed except the increase in intensities of the peaks. This may happen due to the release of the crystal strain during the heat treatment of the alloy. Further increase in heating temperature at 800 ºC (1173K), shows the increase in the intensity of the first

superlattice reflection (100) of the B2 phase, relative to the as-cast structure. This suggests that with increase in heat-treatment temperature degree of ordering increases. It means the volume fraction of the B2 phase is increased. Thermal stability of the evolved phases was further investigated at longer holding time of 12h at 800 ºC (1073K). There was no sign of phase transformation that could be observed even at longer holding time. The diffraction pattern corresponding to this temperature showed all the reflections of the B2 phase. Therefore, it is imperative to say that the B2 type ordered phase is stable over a higher time-temperature range.

Fig. 6.10 shows the diffraction pattern and optical micrograph of the heat-treated sample at 900 ºC (1173 K) for 24h followed by water quenched. No change in the phase structure was observed. However, the splitting in the peaks can be seen at a higher angle. By careful analysis of these two peaks by deconvolution method (c&d), it is confirmed that the two-phase structure of (B2 + BCC) is quite stable at longer holding time as well. In the same line, the morphology of columnar grains is also not affected.

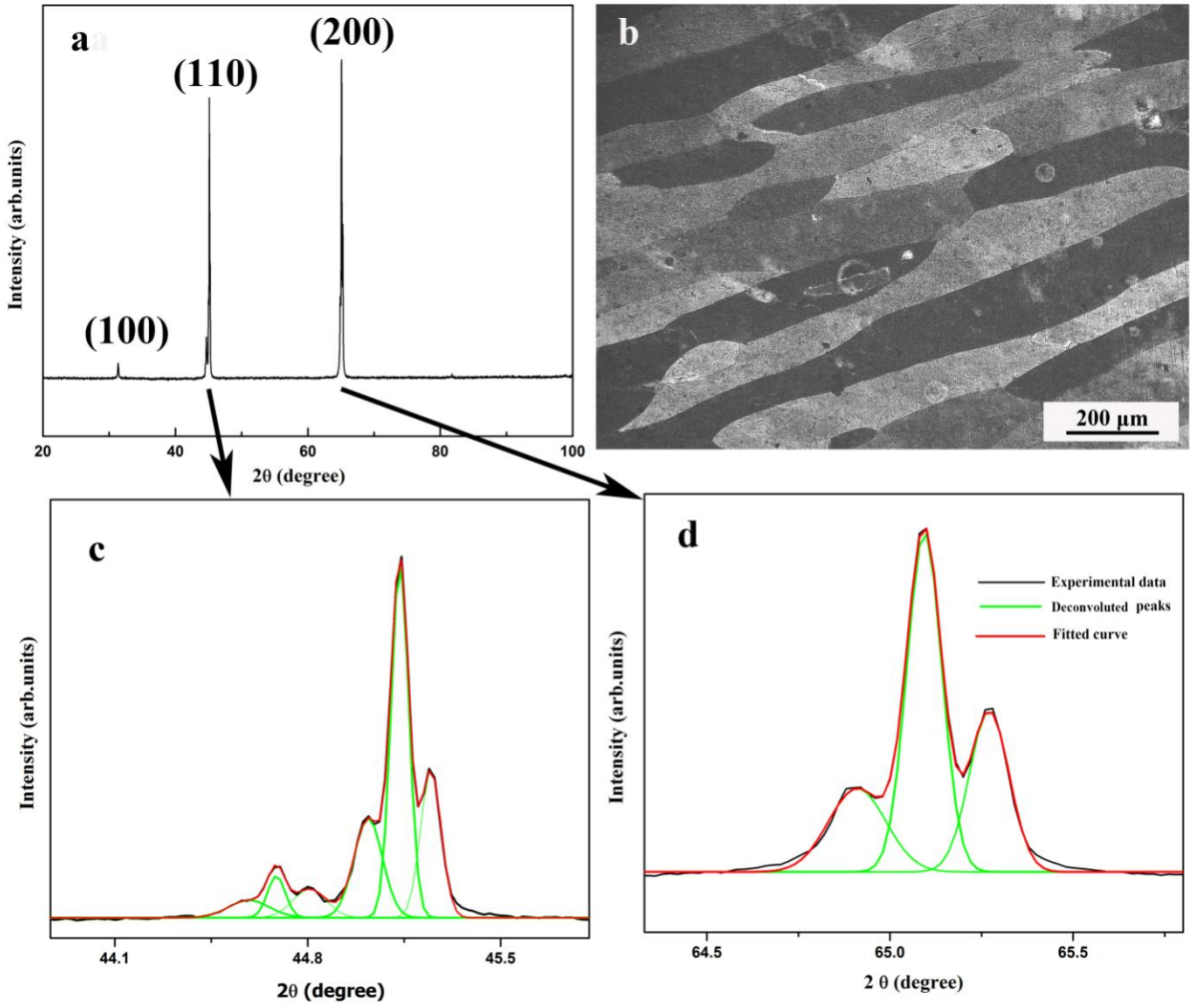

Figure 6.10: X-ray diffraction pattern of (a) heat-treated sample 900 ºC (1173 K) for 24h and then water quenched (b) corresponding optical micrograph of the same sample, (c) & (d) enlarge the view of the two intense peaks, deconvoluted to show the distinct peaks.

6.5 Mechanical behaviour

In order to understand the mechanical behaviour of the as-cast $Fe_{40}Cr_{25}Ni_{15}Al_{15}Co_5$ HEA, the room temperature compression test was performed. The obtained graph of the engineering stress (MPa) and strain (%) is depicted in Fig. 6.11.

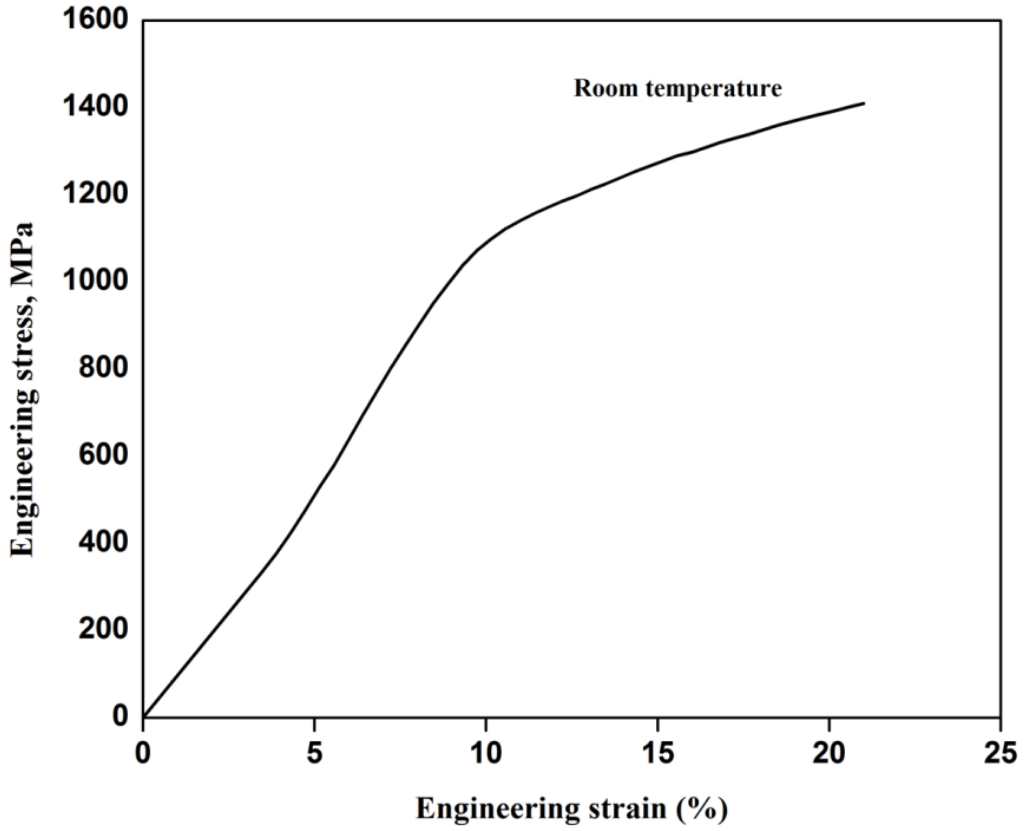

Figure 6.11: Engineering stress-strain curve obtained from the compression test of as-cast $Fe_{40}Cr_{25}Ni_{15}Al_{15}Co_5$ HEA at room temperature.

The alloy is found to have the yield strength of ~ 1012 MPa and ultimate compressive strength of ~1405 MPa. The yield strength of the studied alloy is comparatively higher than some of the earlier reported HEAs, but the alloy lacks in the plasticity. This may be due to the presence of the brittle Ni-Al based B2 type intermetallic phase. The microhardness measurements were performed for the as-cast and heat-treated samples (water quenched) to evaluate the hardness of the alloy. The observed results are listed in Table 6.2. The hardness values decrease with an increase in the annealing temperature, i.e. from ~425 HV to ~390 HV.

Table 6.2: Vickers microhardness (HV) results of $Fe_{40}Cr_{25}Ni_{15}Al_{15}Co_5$ HEA in as-cast and heat-treated samples.

Sample details	Vickers microhardness (HV)
As-Cast	425±5
Heat-treated-873K for 2h	408±5
Heat-treated-1173K for 2h	390±8

6.6 Discussion

The evolution of the phases, thermal stability and mechanical behaviour of the presently investigated alloy can be understood in more details in the following sections.

6.6.1 Phase evolution in as-cast $Fe_{40}Cr_{25}Ni_{15}Al_{15}Co_5$ HEA

The as-cast structure of the $Fe_{40}Cr_{25}Ni_{15}Al_{15}Co_5$ HEA showed the formation of a BCC derived B2 type intermetallic phase enriched in Ni-Al composition. The formation of Ni-Al rich B2 type phase in Fe-Cr rich matrix can be better understood through the thermodynamic point of view. For this purposes, the mixing enthalpies of the binary components in the presently studied alloy were calculated through Miedema model and given in Table 6.3. It could be observed that the mixing enthalpy of the Ni-Al pair is more negative (-22 kJ/mol) compared to the other pairs. Therefore, the studied alloy favours the formation of Ni-Al rich ordered phase. The Ni-Al rich particles are thought to be formed during cooling of the compositionally rich Fe-Cr matrix. The limited solid solubility of the Ni-Al leads to form Ni-Al rich particles in the Fe-Cr rich BCC matrix.

Table 6.3: The calculated values of mixing enthalpy (ΔH_{mix} (kJ/mol)), of atomic pairs for $Fe_{40}Cr_{25}Ni_{15}Al_{15}Co_5$ HEA following Miedema approach.

Elements	Al	Co	Cr	Fe	Ni
Al	-	-19	-10	-11	-22
Co	-19	-	- 4	-1	0
Cr	- 10	- 4	-	-1	-7
Fe	- 11	- 1	- 1	-	-2
Ni	- 22	0	- 7	- 2	-

Apart from the above-mentioned mixing enthalpy, the valence electron concentration (VEC) is also reported to affect the structural evolution [36]. The VEC for the present alloy is 7.1. It is established that the VEC (≥ 8) favors the formation of FCC type solid solution and VEC (≤ 6.87) favors the formation of BCC type solid solution whereas the intermediates values support the formation of mixed FCC & BCC structures. The present calculated value falls in the intermediate range of BCC and FCC [36]. Thus, the VEC criterion does not hold true for the present alloy to predict the structural evolution. As mentioned earlier in the introduction section that the present alloy was designed to understand the role of configuration entropy on phase formation by deviating the typical range of elemental concentration of HEAs (5-35at%). The investigated alloy showed the formation of two-phase structure (B2+BCC); it means the role of configuration entropy is still a decisive factor to form the simple solid solution phases. However, the formation of simple phases is basically governed by binary atomic paring between constituent elements and the competition between entropy and enthalpy for minimizing the Gibbs free energy. Yao et al. [155] have designed the non-equiatomic $Fe_{40}Mn_{27}Ni_{26}Co_5Cr_2$ HEA and reported the formation of a single stable phase of FCC structure. This alloy composition ruled out the necessary criteria for achieving a single-phase solid solution in HEAs. Formation of the equilibrium shape of any precipitates is basically governed by

minimizing the total energy of the state. This includes elastic and interfacial energy of a system [156, 157]. When the sizes of the precipitates are small, then the elastic strain energy induced by the lattice mismatch of precipitate and matrix is less, then the shape is primarily controlled by minimizing the surface area. This will lead to the formation of the spheroidal or ellipsoidal shapes of particles. However, when the precipitates start growing, then the elastic strain energy becomes dominating and relative contribution of both the energies to total energy can be quantified by using the L parameter [122].

$$L = \frac{\varepsilon^2 \ C_{44}\, r}{s} \qquad \text{.....(6.1)}$$

where ε is lattice misfit, C_{44} is elastic constant for matrix, r is the average precipitate size and s is average specific interfacial energy. For the present work the lattice misfit (ε) between BCC and B2 phase is calculated by using the equation of $\varepsilon = 2 \times (a_{B2}\text{-}a_{BCC}) / (a_{B2}+ a_{BCC})$, where a_{B2} and a_{BCC} are the lattice parameters of B2 and BCC phase. The ε & r values for the present alloy is 0.138 % ~ 300 ± 20 nm, respectively. C_{44} and s values for the BCC/B2 are taken from B2-NiAl phase, being 130 GPa and 0.125 J/m^2 respectively. The moderate value of L (0.59) for the present alloy favours the formation of the coherent cuboidal B2 precipitates.

6.6.2 Thermal stability of $Fe_{40}Cr_{25}Ni_{15}Al_{15}Co_5$ HEA

Differential scanning calorimetric (DSC) thermogram of as-cast $Fe_{40}Cr_{25}Ni_{15}Al_{15}Co_5$ HEA showed no major phase transformation event. The minor exothermic event in the temperature range of 400-600ºC was observed. This exothermic event was substantiated by following the annealing treatment at 873K and 1173 K for 2 hours. There was no sign of phase transformation evolved during this thermal treatment.

The only noticeable change is in the intensity of the superlattice reflection peak. This is due to the increase of the volume fraction of the ordered phase. In the same line, the alloy was further annealed at 1073 K for 12h. It has been found that the alloy is thermally stable even at longer holding time. It was further substantiated by heat-treatment at1173K for a longer holding time of 24 h (figure 6.10). High thermal stability is the result of the formation of the precipitation hardening with stronger bonding between unlike pairs of Ni-Al atoms and slower diffusion kinetics (due to the presence of multicomponent) [5].

6.6.3 Mechanical properties of $Fe_{40}Cr_{25}Ni_{15}Al_{15}Co_5$ HEA

The presently investigated alloy showed the mechanical properties (yield strength of ~ 1012 MPa and ultimate compressive strength of ~1405 MPa) comparable to that of the reported HEAs. Zhou et al. [121] have reported the hierarchical nanostructured $Fe_{34}Cr_{34}Ni_{14}Al_{14}Co_4$ HEA with a good combination of high strength (yield strength 1353MPa and fracture strength 2638 MPa) and large plasticity (40.6%). Strengthening mechanism in polycrystalline materials are traditionally governed by four methods: solid solution hardening- associated with point defects in the crystal, grain boundary hardening- associated with planar defects in the crystal, dislocation hardening- associated with line defects and precipitation/dispersion hardening-associated with volumetric defects in the crystal. All these mechanisms are acting independently, so the yield strength of the alloy is a simple summation of the four methods. In the present alloy as the formation of precipitation of secondary particles were observed, it is believed that the excellent mechanical properties of the $Fe_{40}Cr_{25}Ni_{15}Al_{15}Co_5$ HEA are attributed to second phase strengthening mechanism. The formation of the B2 precipitates in BCC matrix has a similar strengthening mechanism in Ni-base superalloys. In Ni-base superalloys, the

cuboidal gamma prime precipitates with $L1_2$ structure (Cu_3Au-type) embedded coherently with FCC gamma matrix. Second phase particles are expected to produce hardening, either through dislocation bypass mechanism (Orowan type) or particle shearing mechanism. In general, Orowan mechanism is valid when the size of the precipitated reaches a critical value or is incoherent with the matrix. However, the shearing mechanism would operate when precipitates are sufficiently small and coherent. Based on the present precipitate morphology, particle shearing mechanism is expected to act as a strengthening mechanism for the current alloy. High hardness values of the HEAs are attributed to the lattice distortion effect, which arises due to the atomic size difference, crystal structure and bonding energy among constituent elements.

6.7 Conclusions

The following conclusion can be drawn from the present investigation:-

(1) A newly designed alloy composition of non-equiatomic $Fe_{40}Cr_{25}Ni_{15}$ $Al_{15}Co_5$ high-entropy alloy was developed successfully by deviation from the equiatomic compositional definition of HEA. The induction melting technique was effective to produce a large amount of this HEA.

(2) Formation of the two-phase structure of Fe-Cr rich BCC and Ni-Al rich ordered B2 phase was observed in the as-cast condition. However, this alloy composition ruled out the prediction of the structures made by valence electron concentration (VEC) for solid solution formation in HEAs. The coexistence of these two phases has been evolved, perhaps due to the phase separation of the single-phase BCC structure.

(3) The shape of coherent B2 precipitate was determined by lattice misfit (ε) which primarily governs the total energy (L) required to form the cuboidal shape. The alloy had good structural stability at different heat-treatment temperature.

(4) The alloy exhibited a good combination of high compression yield strength and hardness, i.e. ~1012 MPa & 428±5 HV respectively, which is a result of precipitation strengthening effect.